J. Math. Biol. (2009) 58:545–559
DOI 10.1007/s00285-008-0211-1

Mathematical Biology

Multiscale agent-based cancer modeling

Le Zhang · Zhihui Wang · Jonathan A. Sagotsky · Thomas S. Deisboeck

Received: 29 March 2007 / Revised: 31 January 2008 / Published online: 12 September 2008
© Springer-Verlag 2008

Abstract Agent-based modeling (ABM) is an in silico technique that is being used in a variety of research areas such as in social sciences, economics and increasingly in biomedicine as an interdisciplinary tool to study the dynamics of complex systems. Here, we describe its applicability to integrative tumor biology research by introducing a multi-scale tumor modeling platform that understands brain cancer as a complex dynamic biosystem. We summarize significant findings of this work, and discuss both challenges and future directions for ABM in the field of cancer research.

Keywords Computational systems biology · Agent-based modeling · Tumor simulation

Mathematics Subject Classification (2000) 37N25

1 Introduction

After years of pioneering work by a relatively small number of groups, the field of computational cancer biology has recently been moved closer to the spotlight due to widely publicized research programs such as the National Cancer Institute's Integrative

L. Zhang · Z. Wang · J. A. Sagotsky · T. S. Deisboeck (✉)
Complex Biosystems Modeling Laboratory,
Harvard-MIT (HST) Athinoula A. Martinos Center for Biomedical Imaging,
Massachusetts General Hospital-East 2301, Bldg. 149, 13th Street, Charlestown, MA 02129, USA
e-mail: deisboec@helix.mgh.harvard.edu

Present Address:
L. Zhang
Department of Mathematical Sciences, Michigan Technological University,
1400 Townsend Drive, Houghton, MI 49931, USA

Cancer Biology Program (http://icbp.nci.nih.gov/) and works that start to come out of it [1]. In this review here, we focus on a particularly promising computational modeling technique that is being used to investigate tumors as complex dynamic biosystems, called *agent-based modeling* or ABM. We start with placing this technique into a broader context by comparing it with other commonly used in silico techniques. This section is then followed by a concrete example where we review the progress that we have been able to make using this technique in modeling malignant brain tumors across multiple scales of interest. We conclude this review by summarizing this technique's merits before we move to discussing future directions.

2 Continuum versus discrete modeling

Generally speaking, mathematical modeling can be classified in *continuum* and *discrete* approaches, as well as so called *hybrids*, which combine both techniques in one form or another. From an in silico oncology perspective, continuum models describe terms like tumor cell density [2–5], chemoattractants, nutrient distribution, and even kinetic molecular pathway networks with a set of differential equations [6,7]. These models employ fluid and continuum mechanic principles to represent mass diffusion and convection in the extracellular matrix or tumor tissue [8–10]. Conversely, a discrete model is commonly represented by a cellular automaton (CA) [11]. Such a CA describes a spatial matrix in which the dynamics are defined by a set of local interaction rules among neighboring 'nodes' that can also decide the transition and communication among the grid points. Unless otherwise stated, we and others usually have each grid point represent an individual agent or a cluster of agents [12–15]. Regardless, due to the inherent complexity of the tumor itself as well as its microenvironment, arguably neither a true continuum nor a mere discrete model can describe all processes sufficiently. For instance, highlighted already by Orme and Chaplain [16] and then referred to by Byrne et al. [17] continuum angiogenesis models cannot account for the discreteness of distinct vascular morphologies, or, e.g. distinguish between anastomosis and capillary tip death. Similarly, a discrete model by itself falls short on investigating most fluid physical aspects of relevance to cancer [18]. Therefore, hybrid models [19,20]—like ABMs—are becoming increasingly popular due to their ability to allow for tumor simulations across multiple scales in space and time [21–23]. In the following section we will describe this technique in more detail.

3 Agent-based modeling

Agent-based modeling (ABM) is a computational technique that simulates the (inter) actions of autonomous individuals ('agents') within a complex system. Each agent is encoded with a set of pre-specified rules, so that it can individually execute a series of operations and make decisions. ABM is the technique of choice to investigate emergent patterns in *complex dynamic systems* [24].

In practice, ABM has been used to approach a variety of business and technology problems since the mid-1990s. Such 'use cases' include for (a) *Social Sciences*,

ABSS, an agent based social simulation system that is commonly employed to study e.g. the consequence of a particular social policy [25]; for (b) *Economics*, the fact that the dynamics of a business result from the behavior of many interacting customers, hence making ABM a natural choice to reflect these entities properly. Here, one widely reported commercial ABM application was developed by Bios Group for the NASDAQ Stock Market and was geared towards simulating the impact of regulatory changes on the financial market [26]; for (c) *Transportation Management*, the ABM package TRansportation Analysis SIMulation System (TRANSIMS; http://transims.tsasa.lanl.gov/) which has been developed at Los Alamos National Laboratory to simulate the movements of individual vehicles on a regional transportation network and to estimate air pollution emission generated by vehicle movements; and finally for (d) *Life Sciences*, for instance 'Evo' (http://omicrongroup.org/evo/), an ABM framework used to model genetic recombination and mutations. In addition, other ABM Life Sciences applications range from more general biomedicine [27,28] and immunology [29–31] to clinical trial simulation [32,33] and in silico oncology [12–14,21–23,27,34,35]. In the next section, we will now describe the use of ABM for cancer modeling in more detail.

Several recent oncology applications of ABM focus on simulating growth dynamics of multicellular tumor spheroids (MTS). For instance, Schaller and Meyer-Hermann [36] developed a three dimensional agent-based Voronoi-Delaunay hybrid model. The authors compared the simulation results with experimental tumor growth data in an effort to test the hypothesized functional dependence of the uptake rates of two nutrients, glucose and oxygen, and to find suitable mechanisms for the induction of necrosis. Engelberg et al. [37] built up another ABM model consisting of different spaces for tumor cells, oxygen, nutrient and toxic inhibitors to simulate the general structure of MTS as well as the patterns of the relative time course of spheroid growth. Zhu et al. [38] then established a three dimensional biophysical ABM to study the self-assembly of MTS. Their results indicate that MTS will not form if the adhesion coefficient between the tumor cells is much smaller than the adhesion coefficient between cells and substrate. Using another ABM, Spencer et al. [39] modeled tumor progression with a small set of underlying rules that govern the transformation of normal cells to cancerous cells. In our group, we have pioneered the use of ABM to simulate cancer *across multiple scales in space and time*, by integrating molecular pathway dynamics with *both* microscopic cell behavior and multicellular or macroscopic expansion patterns [12–14,21–23,34]. The next section reviews this work.

4 Agent-based modeling of brain tumors

Over the years, we have developed a variety of ABM that focus on simulating highly malignant brain tumors as *complex dynamic, self-organizing biosystems*. This approach requires not only a representation of the tumor itself but also a more detailed description of the virtual microenvironment. Extending the traditional CA framework to ABM we not only model both time and space *discretely*, but also treat a number of the biological components of interest as *continuum* variables, thus avoiding the need to transform these variables into unrealistic integer states (as in a more traditional CA model). The

result is a *hybrid, multiscale* ABM algorithm. The following sections give an overview over the details involved.

4.1 Macroscopic–microscopic scales

Following a 'top-down' approach, in [34] we have introduced a two-dimensional (2D) ABM in which tumor cells can proliferate, migrate, turn quiescent, or undergo cell death. The extracellular matrix of the model is set up as a 2D torus grid lattice of 50×50 locations that represent a virtual brain tissue slice. Nutrient sources, mechanical confinement (representing biomechanical tissue properties that resist tumor expansion) and toxic metabolites are initialized at each location by normal distribution, denoted in Eq. 1, with the highest replenished nutrient source set up in the center of quadrant three ('North') of the lattice (see Fig. 1a).

$$X_j = T_m \exp(-2d_{ij}^2/\sigma_t^2) \tag{1}$$

Here X_j represents the concentration of a chemoattractant at each location, T_m stands for the constant value of that attractant, and d_{ij} is the distance between location, i, of the highest nutrient value (i.e., source) and the tumor cell's current location, j. The alterations of the tumor cell population through proliferation and cell death are expressed in Eqs. 2 and 3

$$\mathrm{Pr}_{\mathrm{proliferate},j} = \varphi_j/(k_\varphi + \varphi_j), \tag{2}$$

where k_φ is a parameter constant and φ_j is the nutrient concentration at location j. The probability of a given cell to proliferate ($\mathrm{Pr}_{\mathrm{proliferate},j}$) is diminished when nutrient supply is scarce. Similarly, cell death is more likely in lattice areas with comparably high levels of hypoxia and cytotoxic factors such as lysosomes, set free by perishing bystander cells. This is expressed in

$$\mathrm{Pr}_{\mathrm{death},j} = \tau_j/(k_\tau + \tau_j), \tag{3}$$

where k_τ is another parameter constant, τ_j stands for the level of toxicity at location j and $\mathrm{Pr}_{\mathrm{death},j}$ is the probability of a given cancer cell to die. At every time step each cell takes up nutrients and generates detrimental byproducts on site, according to Eqs. 4 and 5, respectively.

$$\varphi_{t,j} = \varphi_{t-1,j} - r_\varphi l_{t-1,j} \tag{4}$$

$$\tau_{t,j} = \tau_{t-1,j} + r_\tau l_{t-1,j} \tag{5}$$

Additionally, at each time step, when a tumor cell is eligible to migrate or proliferate into a new location, it employs a chemotactic *search* mechanism that enables the cell to rank the attractiveness of its surrounding neighborhood. In [34] we had proposed two search algorithms, 'global' and 'local', describing how two differentially sensitive

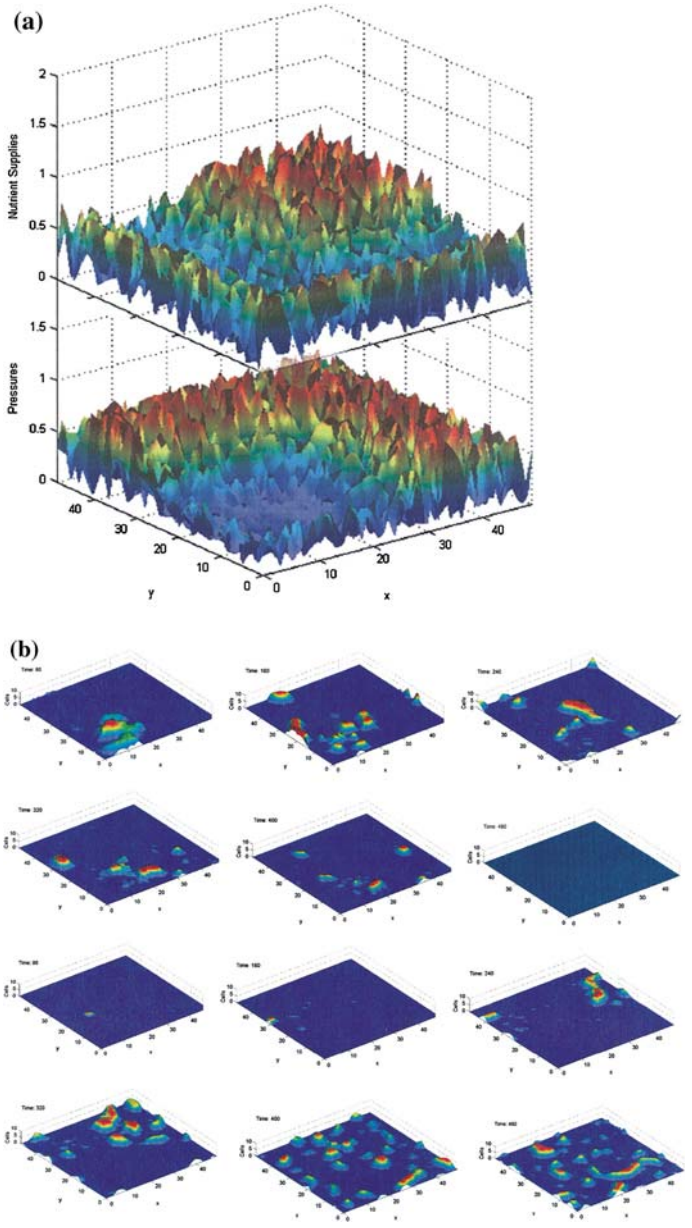

Fig. 1 **a** Depicts the distribution of nutrients (*top*) versus the profile of mechanical confinement (*bottom*) in a 2D lattice space that is divided into four quadrants: frontal (*south*) as quadrant I, right (*east*) as II, distal (*north*) as III, and left (*west*) as IV. **b** The top six snapshots describe the tumor cluster patterns resulting over time when 'global' chemotactic search is dominant, whereas the bottom six simulation snapshots show the emergent patterns when 'local' chemotactic search prevails. The images are taken at time step $t = 0$, 80, 160, 240, 320, and 400 (arbitrary units). The *rainbow color scale* represents the density of viable tumor cells per cluster (from Mansury et al. [34]) (For color format, please visit the online version of the article)

cell-surface receptors would process a given cell's chemotactic movement by utilizing two distinct intracellular amplification strengths. That is, the cell-surface receptor for global search has a lower signal detection threshold rendering it more sensitive to even faint diffusive signals emitted from a distant location. On the contrary, the receptor for local search is employed to receive the stronger signals from the local neighborhoods of the cell's current location hence can afford a less sensitive signal detection threshold. This initially rather simple ABM yields a rather intriguing finding: the emergence of a *phase transition* that leads to two distinct spatiotemporal patterns depending on the dominant search mechanism. That is, if global search plays a more prominent role, it will result in an invasive tumor system that operates with a few large cell clusters and that expands rapidly yet, as a tradeoff, seems to have a limited lifetime. In contrast, the use of more local search generates a tumor system that operates with many small cell clusters with longer lifetime, but at a somewhat slower spatiotemporal expansion rate. Figure 1b shows the simulation results of this 2D tumor model which, at least for the in silico situation, supported the argument of a link between a cancer system's multicellular *structural pattern* and its *functional performance*. Extending this work, in [12] we have studied the tumor system's behavior under local search only, now varying the level of search *precision* by introducing a noise function into the previous search mechanism as seen in Eq. 6.

$$T_j = \psi \cdot L_j + (1 - \psi) \cdot \varepsilon_j \tag{6}$$

Here T_j denotes the attractiveness of location j, L_j is the error-free evaluation of location j, and $\varepsilon_j \sim N(\mu, \sigma^2)$ is an error term that is normally distributed with mean μ and variance σ. The parameter ψ takes on a positive value between zero and one and represents the extent of search precision. As a concrete example, a 70% search precision implies that $\text{Prob}[T_j = L_j] = 0.7$, i.e., the attractiveness of location j is evaluated by the tumor cell without mistake in seven out of ten trials on average. At one extreme, $\psi = 1$ represents the situation in which tumor cells consistently evaluate the permissibility of a location without error, hence behave fully chemotactically *biased*. At the other extreme, $\psi = 0$ represents the case when tumor cells always perform a *random walk* motion, in a sense, completely ignore the guidance of the gradients of environmental cues. This study also depicted a much more complicated ECM than the previous iteration [34] by incorporating the diffusion of toxic metabolites and nutrients as well as a mechanical resistance reduction. The numerical results of this extended ABM reveal that multicellular tumor systems not only are not slowed down by a moderate level of processing errors, rather, they may be able to even exploit an in vivo presumably rather "noisy" micro-environment, since a less than perfect search can yield the fastest spatiotemporal expansion (see Fig. 2). Investigating then a potential relationship between the tumor's surface patterns and the average velocity of its spatial expansion, in [13] we report that "while the time-series behavior of the structural patterns of the growing tumor and the extent of its tumor-stromal border invasion are largely uncorrelated, there however is a strong correlation between the increase of the so called "beaten-path advantage" (the tendency of cells to follow others (which can be thought of as a implicit representation of e.g. the cell's matrix-

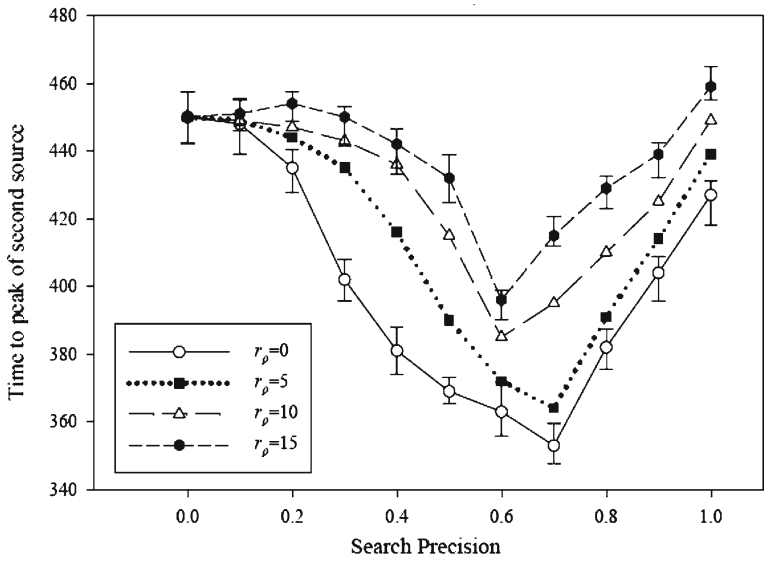

Fig. 2 Shows the time (y-axis) that it takes the first tumor cell to reach the nutrient source in the NE quadrant versus the chemotactic search precision (x-axis) employed, for a variety of different migration capabilities (inversely related to r_ρ). Note that, for this setup, the spatially most aggressive cancer system operates with a search 'precision' that is *less* than perfect (i.e., ∼0.7) (from Mansury et al. [12])

degrading activity)) and an increase in the tumor system's fractal dimension which in turn accelerates the system's overall spatial expansion (see Fig. 2 in [13]).

4.2 Macroscopic–microscopic–molecular scales

Based on these previous developments, in [14] we then began to introduce a *molecular* perspective by incorporating gene expression dynamics into the prior, primarily 'macroscopic–microscopic' framework. Specifically, we investigated the impact of the expression of the genes Tenascin C and proliferating cell nuclear antigen or PCNA on macroscopic brain tumor growth patterns. The numerical results confirm that gene expression of Tenascin C is indeed consistently higher in the migratory glioma cell phenotype whereas the expression of PCNA is consistently higher among proliferating tumor cells. To analyze the time series of Tenascin C and PCNA expression in distinct sub-regions of the tumor, we had employed Detrended Fluctuation Analysis (DFA) [40–44]. The DFA results reveal that correlations between the tumor's macroscopic pattern and its molecular-level gene expression dynamics depend on both the timing and geography of the sampling (see Table 3 in [14]). Furthermore, partitioning the tumor into distinct geographic regions of interest (ROI; using a box counting method [45]) suggests that the gene expression profile of tumor cells in the quadrant closest to the nutrient-abundant region is representative of the entire tumor whereas the expression profile of tumor cells in the geographically opposite ROI is not. While this work did succeed in implementing a molecular scale within such an ABM platform, the gene

expression dynamics herein could not yet directly impact the tumor cell's phenotypic switch and thus failed to influence microscopic behavior.

To address this shortcoming, in [21] we have then explicitly simulated the impact of a molecular 'decision-process' on both the cellular phenotype *and* the emergent multicellular patterns in brain tumors. Focusing on the epidermal growth factor receptor, EGFR, which has been shown to be involved in carcinogenesis in a variety of tumor types, the algorithm ran in 2D and introduced the EGFR ligand, transforming growth factor alpha (TGF_α), to the micro-environment representation in an effort to model autocrine and paracrine cell signal transduction. This study presents a novel computational model in that it truly encompasses molecular, microscopic and macroscopic scales. It incorporated a simplified EGFR pathway representation and utilized PLC_γ to *decide* the cancer cell's phenotype. The latter was inspired by experimental data [46] that argue for a dichotomy in glioma cell behavior in that the same cell is engaging in either proliferation or migration, yet not both traits at the same time. By introducing an implicit treatment of a cell cycle, this ABM iteration exhibits multiple time scales in cell proliferation and migration as well as in the underlying molecular pathway. The simulation results reveal that decreasing the cellular phenotypic decision threshold of PLC_γ results in faster multicellular tumor expansion driven by more migratory behavior (Fig. 3). Most importantly, the in silico results led to rather

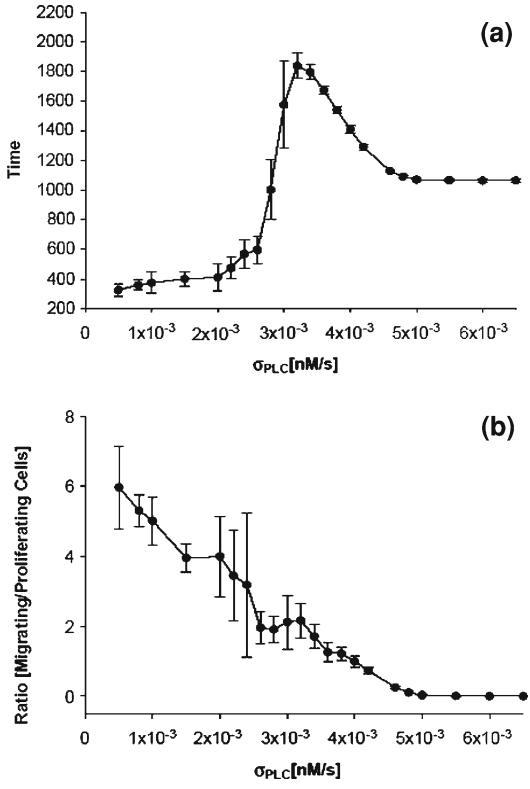

Fig. 3 Describes the impact of varying σ_{PLC} (x-axis) (**a**) on the time (min) it takes the first migratory tumor cell to reach the source of glucose in the NE quadrant (y-axis), and (**b**) on the ratio of migrating to proliferating cells (y-axis) within the expanding cancer system. The *error bars* show the standard deviation between 10 runs using different random number seeds (from Athale et al. [21])

intriguing experimentally testable hypotheses, such as spatial cytosolic polarization of PLC_γ towards an extrinsic chemotactic gradient and the role of PLC_γ in phenotype switching per se. In our subsequent research using this ABM framework, we reported in [22] that increasing the cells' EGF receptor density results in an acceleration of the tumor system's spatiotemporal expansion dynamics (Fig. 4) which, in fact, is already supported by a number of experimental works [47–50].

In preparation of applying these types of ABM algorithms to clinical data, recently Zhang et al. [23] built up a three dimensional (3D) brain cancer modeling algorithm. This iteration now incorporates a rather sophisticated iteration of the EGFR intracellular signaling pathway as well as an explicit cell cycle description (modified from Alarcon et al. [51]) on the molecular scale while continuing to couple its dynamics with the microscopic and macroscopic behavioral levels. Due to its unique design, this model will allow us to not only study how molecular perturbations percolate across scales in space and time, but, properly extended, it can also be used for both carrying out the necessary high performance compute simulations as well as data analysis required to bringing this approach into the clinical arena. For example, alterations within the profile of the EGFR *gene–protein interaction network* (Fig. 5a) can induce a single cancer cell's phenotypic switch locally which in turn can potentially impact invasion directionality and speed on a multicellular level (see Fig. 5b–d for representative simulation results). The workflow of this model is briefly explained as follows:

1. First, the 3D lattice contains $100 \times 100 \times 100$ locations which represent the slice volume of virtual brain tissue in which the concentrations of the chemoattractants, glucose, TGF_α and oxygen are normally distributed. Also, a blood vessel is located at (75, 75, 75) and serves as a replenishing source for these chemical cues.

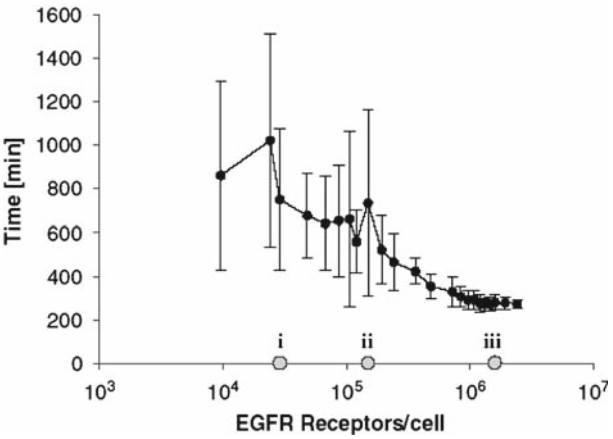

Fig. 4 Plotted is again the time (y-axis) that it takes the first tumor cell to reach the nutrient source versus the number of EGFR receptors per cell (x-axis). The gray circles on the x-axis depict the increasing EGF-receptor densities of (*i*) 2.9×10^4, (*ii*) 1.5×10^5 and (*iii*) 1.59×10^6 per cell, as reported by Lund-Johansen et al. [47] for three human glioma cell lines: (*i*) D-263MG, (*ii*) D-247MG, and (*iii*) D-37MG. The *error bars* result from 23 runs with different random number seeds (from Athale and Deisboeck [22])

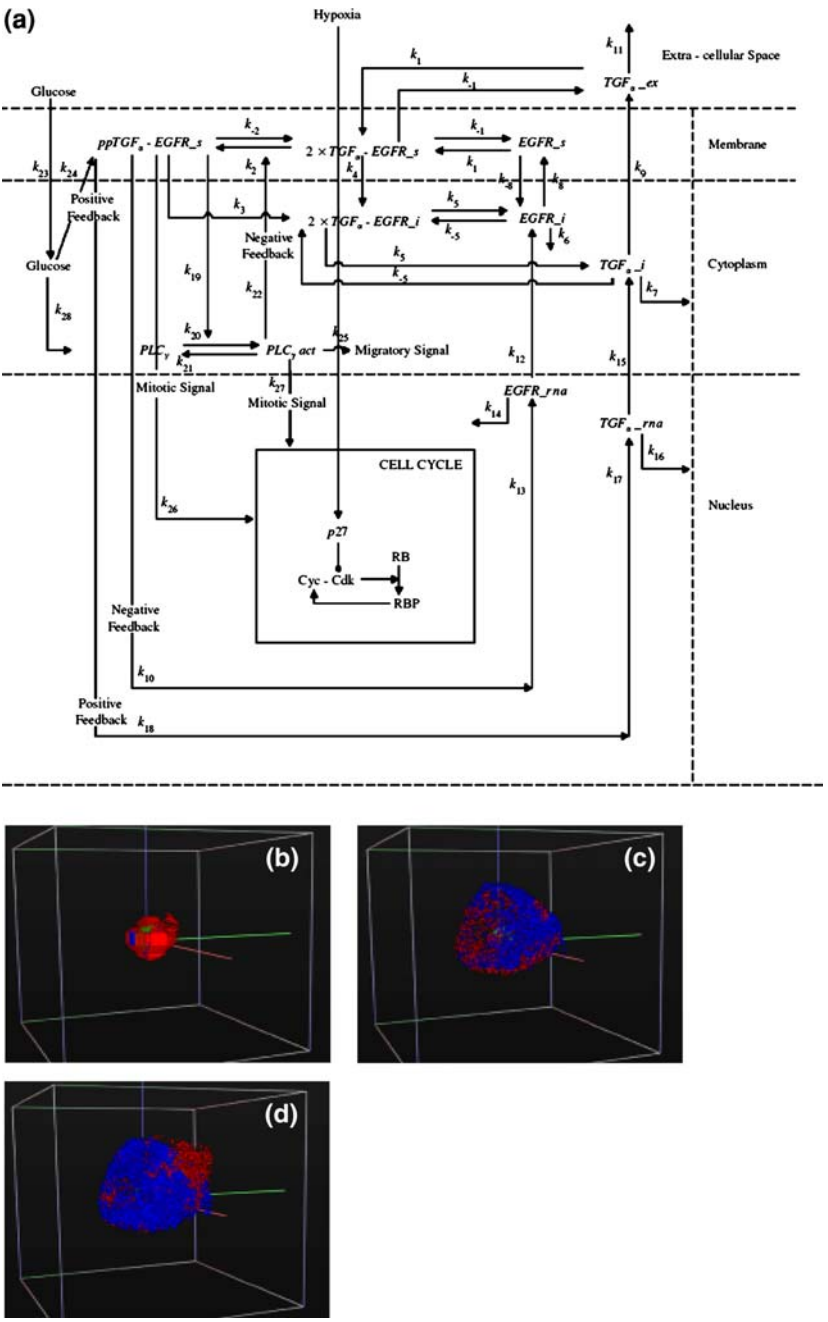

Fig. 5 The diagram depicts the sub-cellular EGFR gene–protein interaction network that spans cell nucleus, cytoplasm and membrane compartments (**a**). The 3D simulation snapshots show the evolving multicellular tumor system at time step $t = 50$ (**b**), $t = 88$ (**c**), $t = 107$ (**d**). Note that proliferative cancer cells are shown in *blue*, migratory cells in *red* (from Zhang et al. [23]) (For color format, please visit the online version of the article)

2. Next, we initialize approximately 500 agents or cancer cells in the center of the 3D lattice, each of which is equipped with the type of EGFR gene–protein network detailed in Fig. 5a.
3. At every simulation step, each cell is 'checked' or updated according to the following rules:
   - 3.1 If the glucose concentration is lower than a set cell death threshold, the cell enters into apoptosis.
   - 3.2 If the glucose concentration is between this cell death and a set quiescent threshold, the cell turns quiescent, a reversible state.
   - 3.3 If the glucose concentration is higher than this quiescent threshold, the cell utilizes the values of the components of its EGFR gene–protein interaction network to process the 'phenotypic decision':
   - 3.3.1 If the cell is in a migratory state (a PLC_γ concentration change over time higher than a set migration threshold) it moves into an unoccupied, neighboring site that harbors the highest glucose concentration. If the entire neighborhood is occupied, the cell turns quiescent until some space frees up.
   - 3.3.2 If the cell is in a proliferative state (a PLC_γ concentration change over time higher than a set proliferation threshold), it runs through its cell cycle at a speed that is correlated with the available oxygen concentration. After completing its cell cycle which, in the model, varies between 22 and 26 h, the cell chooses an empty neighborhood with the highest glucose concentration to replicate and to place its offspring. And, again, if no unoccupied neighboring space can be found, this cell turns quiescent until space becomes available.
4. At the end of each simulation step, the chemoattractants are replenished by the nutrient source and diffuse across the virtual brain slice volume.
5. When the first cell (migratory or proliferative) enters the location of the vessel (75, 75, 75), the simulation is terminated.

Currently, we are expanding this work to model *genetic instability* and the emergence of multiple tumor cell clones (Zhang et al. [52]; results at different simulation time steps are shown in Fig. 6). This advanced 3D ABM is capable of simultaneously modeling five different cancer cell clones, with varying EGFR density. That setup allows us to implement a simplified glioma *progression pathway* that leads from a low malignant brain tumor clone with comparably limited EGFR density up to a highly aggressive clone with increasing EGFR density, thereby properly reflecting experimental and clinical knowledge [53–55]. This iteration also introduced a new phenotypic trait to the model, i.e. tumor cell 'adhesion' that is being coupled to the EGFR density of the cancer cell. We can now begin to link discretely the cells' phenotype to their mutation status, for distinct geographic sub-regions within a growing neoplasm. This is a crucial prerequisite for moving these types of models eventually also into the clinical area where, for patient-specific *predictive* purposes, they could be used to help *integrate*, e.g. the molecular information from biopsy snapshots into consecutively acquired MR-imaging lattices.

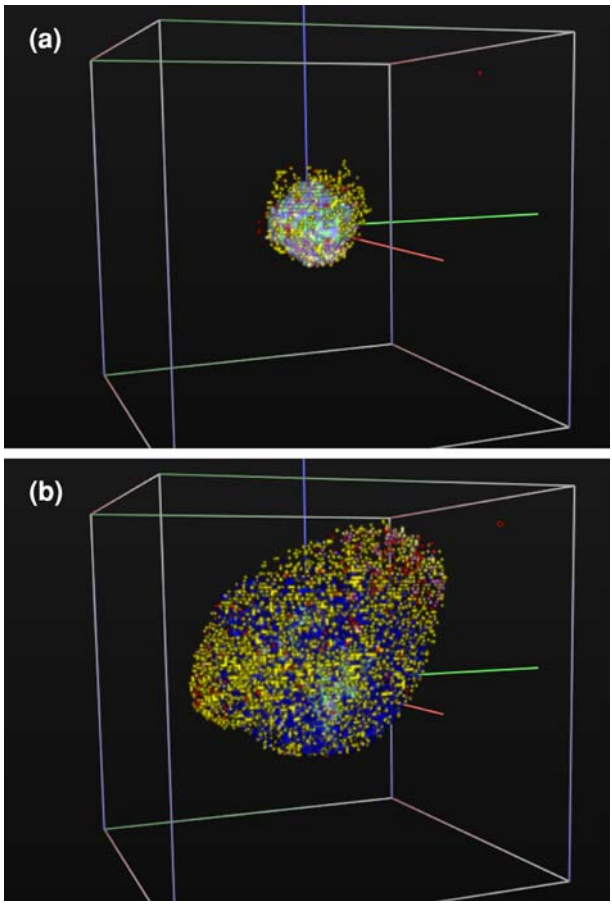

Fig. 6 Displayed are 3D snapshots of a polyclonal brain tumor system at time step $t = 110$ (**a**), and $t = 225$ (**b**). The *red circle* in the third quadrant of the 3D cube depicts the location of the 'virtual' blood vessel which serves as a replenished nutrient source. Representing a simplified tumor progression pathway, the color shades relate to five (5) glioma cell clones (that differ in their increasing amount of EGFR density and decreasing extent of tumor cell–tumor cell adhesion) and their alternating four (4) phenotypes (proliferation, migration, quiescence and apoptosis (the latter two traits are displayed in *gray* and *black colors*, for all clones)) (Zhang et al. [52]) (For color format, please visit the online version of the article)

5 Summary and future work

As illustrated by the example above, agent-based tumor modeling has several significant advantages that should accelerate its dissemination throughout the computational cancer biology community [56]: (1) ABM is a natural representational formalism. Because of this characteristic feature, a cancer cell's biological property and behavior can be well defined with ABM. This enhances the model's biological relevance; (2) ABM can simulate and allows analyzing emergent properties of a biosystem such as cancer; (3) ABM is flexible, hence can be employed in multiple dimensions. In other words, it is *scalable* which is essential for its applicability in a clinical context.

ABM has particular relevance for computational cancer biology [26] since: (1) the interactions between the agents (i.e., cells, proteins, and/or genes) are nonlinear, discontinuous, and discrete; (2) space is crucial and the agents' positions are not fixed; (3) the agents' population is heterogeneous, and each individual species is different, at least to some degree, as a consequence of tumor progression; (4) the topology of all these interactions is complex.

Despite its applicability for the problem at hand, admittedly, ABM still has some drawbacks. For instance, since ABM describes the system at the level of its constituent units but not at the top level, its computational demand, at biomedically relevant scales, can already be significant and will only increase given the amount of data forthcoming from genomics and proteomics as well as clinical imaging studies. For the moment, moving 3D ABMs onto parallel computing platforms should be an efficient way to address this issue by separating the computing workload over a grid of several thousand processors. Eventually, however, the shear volume of data such multiscale modeling platforms have to handle, particularly at the molecular level, will require more creative solutions. Guided by the concept to employ compute resources in a simulation run where and when they are needed the most we and others have been moving into the direction of multi-scale, *multi-resolution* modeling of tumors. This route, while arguably very promising, proves to be equally challenging, given the range of data to deal with and the computational techniques required. The latter includes the use of grid-enabled environments, semantic data repositories, and analytic web-services in conjunction with novel workflow design—to a large degree all still in their developmental stage, certainly for the Life Sciences arena. It is here where innovative multi-institutional efforts, such as the National Cancer Institute's *Center for the Development of a Virtual Tumor* (CViT; http://www.cvit.org) are poised to have an impact. Charged with developing the first international community of cancer modelers, and the innovative infrastructure to support it, CViT has the potential to become a much needed, vibrant test bed and launching pad for these new technologies and thus a critical enabler for multi-scale and multi-resolution cancer modeling.

In summary, agent-based modeling represents a most valuable computational technique, which will allow us, at an ever increasing resolution, to simulate cancer across multiple scales of interest in both space and time. Its modeling results help generating experimentally testable hypotheses, allow for data integration, and, if properly expanded, will prove useful for predictive purposes in clinics both on the diagnostic and therapeutic side.

Acknowledgments This work has been supported in part by NIH grants CA 085139 and CA 113004 and by the Harvard-MIT (HST) Athinoula A. Martinos Center for Biomedical Imaging and the Department of Radiology at Massachusetts General Hospital.

References

1. Anderson AR, Weaver AM, Cummings PT, Quaranta V (2006) Tumor morphology and phenotypic evolution driven by selective pressure from the microenvironment. Cell 127:905–915
2. Swanson KR, Alvord EC Jr, Murray JD (2000) A quantitative model for differential motility of gliomas in grey and white matter. Cell Prolif 33:317–329

3. Swanson KR, Alvord EC Jr, Murray JD (2002) Virtual brain tumours (gliomas) enhance the reality of medical imaging and highlight inadequacies of current therapy. Br J Cancer 86:14–18
4. Swanson KR, Alvord EC Jr, Murray JD (2002) Quantifying efficacy of chemotherapy of brain tumors with homogeneous and heterogeneous drug delivery. Acta Biotheor 50:223–237
5. Swanson KR, Bridge C, Murray JD, Alvord EC Jr (2003) Virtual and real brain tumors: using mathematical modeling to quantify glioma growth and invasion. J Neurol Sci 216:1–10
6. Araujo RP, Petricoin EF, Liotta LA (2005) A mathematical model of combination therapy using the EGFR signaling network. Biosystems 80:57–69
7. Armstrong NJ, Painter KJ, Sherratt JA (2006) A continuum approach to modelling cell–cell adhesion. J Theor Biol 243:98–113
8. Zhang L, Dai W, Nassar R (2005) A numerical method for optimizing laser power in the irradiation of a 3D triple layered cylindrical skin structure. Numer Heat Tr A 48:21–41
9. Zhang L, Dai W, Nassar R (2006) A numerical method for obtaining an optimal temperature distribution in a 3D triple-layered cylindrical skin structure embedded with a blood vessel. Numer Heat Tr A 49:765–784
10. Chaplain M, Lolas G (2005) Mathematical modelling of cancer cell invasion of tissue: The role of the urokinase plasminogen activation system. Math Modell Methods Appl Sci 15:1685–1734
11. Wolfram S (1994) Cellular automata and complexity: collected papers. Addison-Wesley, Reading, MA
12. Mansury Y, Deisboeck TS (2003) The impact of "search precision" in an agent-based tumor model. J Theor Biol 224:325–337
13. Mansury Y, Deisboeck TS (2004) Simulating 'structure-function' patterns of malignant brain tumors. Physica A 331:219–232
14. Mansury Y, Deisboeck TS (2004) Simulating the time series of a selected gene expression profile in an agent-based tumor model. Physica D 196:193–204
15. Schofield P, Chaplain M, Hubbard S (2005) Evolution of searching and life history characteristics in individual-based models of host-parasitoid-microbe associations. J Theor Biol 237:1–16
16. Orme ME, Chaplain MA (1997) Two-dimensional models of tumour angiogenesis and anti-angiogenesis strategies. IMA J Math Appl Med Biol 14:189–205
17. Byrne HM, Alarcon T, Owen MR, Webb SD, Maini PK (2006) Modelling aspects of cancer dynamics: a review. Philos Transact A Math Phys Eng Sci 364:1563–1578
18. Kansal AR, Torquato S, Harsh IG, Chiocca EA, Deisboeck TS (2000) Cellular automaton of idealized brain tumor growth dynamics. Biosystems 55:119–127
19. Anderson AR, Chaplain MA (1998) Continuous and discrete mathematical models of tumor-induced angiogenesis. Bull Math Biol 60:857–899
20. Anderson AR, Chaplain M, NewMan EL, Stelle RJC, Thompson AM (2000) Mathematical modelling of tumor invasion and metastasis. J Theor Med 2:129–154
21. Athale C, Mansury Y, Deisboeck TS (2005) Simulating the impact of a molecular 'decision-process' on cellular phenotype and multicellular patterns in brain tumors. J Theor Biol 233:469–481
22. Athale CA, Deisboeck TS (2006) The effects of EGF-receptor density on multiscale tumor growth patterns. J Theor Biol 238:771–779
23. Zhang L, Athale CA, Deisboeck TS (2007) Development of a three-dimensional multiscale agent-based tumor model: simulating gene–protein interaction profiles, cell phenotypes and multicellular patterns in brain cancer. J Theor Biol 244:96–107
24. Sanga S, Sinek JP, Frieboes HB, Ferrari M, Fruehauf JP, Cristini V (2006) Mathematical modeling of cancer progression and response to chemotherapy. Expert Rev Anticancer Ther 6:1361–1376
25. Davidsson P (2002) Agent based social simulation: a computer science view. JASSS 5
26. Bonabeau E (2002) Agent-based modeling: methods and techniques for simulating human systems. Proc Natl Acad Sci USA 99(Suppl 3):7280–7287
27. Moreira N (2006) In pixels and in health: computer modeling pushes the threshold of medical research. Sci News 169:40–41
28. Peirce SM, Van Gieson EJ, Skalak TC (2004) Multicellular simulation predicts microvascular patterning and in silico tissue assembly. FASEB J 18:731–733
29. Kirschner D, Panetta JC (1998) Modeling immunotherapy of the tumor–immune interaction. J Math Biol 37:235–252
30. Perrin D, Ruskin HJ, Crane M (2006) An agent-based approach to immune modelling: priming individual response. Trans Eng Comput Technol 17:80–86

31. Segovia-Juarez JL, Ganguli S, Kirschner D (2004) Identifying control mechanisms of granuloma formation during *M. tuberculosis* infection using an agent-based model. J Theor Biol 231:357–376
32. An G (2001) Agent-based computer simulation and sirs: building a bridge between basic science and clinical trials. Shock 16:266–273
33. An G (2004) In silico experiments of existing and hypothetical cytokine-directed clinical trials using agent-based modeling. Crit Care Med 32:2050–2060
34. Mansury Y, Kimura M, Lobo J, Deisboeck TS (2002) Emerging patterns in tumor systems: simulating the dynamics of multicellular clusters with an agent-based spatial agglomeration model. J Theor Biol 219:343–370
35. Wodarz D, Komarova NL (2005) Computational biology of cancer. World Scientific Publishing Company, Singapore
36. Schaller G, Meyer-Hermann M (2005) Multicellular tumor spheroid in an off-lattice Voronoi-Delaunay cell model. Phys Rev E Stat Nonlin Soft Matter Phys 71:051910
37. Engelberg J, Ganguli S, Hunt CA (2006) Agent-based simulations of in vitro multicellular tumor spheroid growth. In: Proceedings of the agent-directed simulation symposium, pp 141–148
38. Zhu JJ, Coakley S, Holcombe M, MacNeil S, Smallwood RH (2006) Individual cell-based simulation of 3D multicellular spheroid self-assembly. Eur Cells Mater 11(Suppl 3):31
39. Spencer SL, Gerety RA, Pienta KJ, Forrest S (2006) Modeling somatic evolution in tumorigenesis. PLoS Comput Biol 2:e108
40. Buldyrev SV, Goldberger AL, Havlin S, Peng CK, Stanley HE, Stanley MH, Simons M (1993) Fractal landscapes and molecular evolution: modeling the myosin heavy chain gene family. Biophys J 65:2673–2679
41. Hausdorff JM, Peng CK, Ladin Z, Wei JY, Goldberger AL (1995) Is walking a random walk? Evidence for long-range correlations in stride interval of human gait. J Appl Physiol 78:349–358
42. Ossadnik SM, Buldyrev SV, Goldberger AL, Havlin S, Mantegna RN, Peng CK, Simons M, Stanley HE (1994) Correlation approach to identify coding regions in DNA sequences. Biophys J 67:64–70
43. Peng CK, Buldyrev SV, Havlin S, Simons M, Stanley HE, Goldberger AL (1994) Mosaic organization of DNA nucleotides. Phys Rev E Stat Phys Plasmas Fluids Relat Interdiscip Topics 49:1685–1689
44. Peng CK, Havlin S, Stanley HE, Goldberger AL (1995) Quantification of scaling exponents and crossover phenomena in nonstationary heartbeat time series. Chaos 5:82–87
45. Barabasi AL, Stanley HE (1995) Fractal concepts in surface growth. Cambridge University Press, Cambridge
46. Giese A, Loo MA, Tran N, Haskett D, Coons SW, Berens ME (1996) Dichotomy of astrocytoma migration and proliferation. Int J Cancer 67:275–282
47. Lund-Johansen M, Bjerkvig R, Humphrey PA, Bigner SH, Bigner DD, Laerum OD (1990) Effect of epidermal growth factor on glioma cell growth, migration, and invasion in vitro. Cancer Res 50:6039–6044
48. Lund-Johansen M, Forsberg K, Bjerkvig R, Laerum OD (1992) Effects of growth factors on a human glioma cell line during invasion into rat brain aggregates in culture. Acta Neuropathol 84:190–197
49. Schlegel J, Merdes A, Stumm G, Albert FK, Forsting M, Hynes N, Kiessling M (1994) Amplification of the epidermal-growth-factor-receptor gene correlates with different growth behaviour in human glioblastoma. Int J Cancer 56:72–77
50. Westermark B, Magnusson A, Heldin CH (1982) Effect of epidermal growth factor on membrane motility and cell locomotion in cultures of human clonal glioma cells. J Neurosci Res 8:491–507
51. Alarcon T, Byrne HM, Maini PK (2004) A mathematical model of the effects of hypoxia on the cell-cycle of normal and cancer cells. J Theor Biol 229:395–411
52. Zhang L, Wang Z, Sagotsky JA, Deisboeck TS (2008) Simulating brain tumor heterogeneity with a multiscale agent-based model: linking molecular signatures, phenotypes and expansion rate. Math Comput Model. doi:10.1016/j.mcm.2008.05.011
53. Kleihues P, Ohgaki H (1999) Primary and secondary glioblastomas: from concept to clinical diagnosis. Neuro Oncol 1:44–51
54. Lang FF, Miller DC, Koslow M, Newcomb EW (1994) Pathways leading to glioblastoma multiforme: a molecular analysis of genetic alterations in 65 astrocytic tumors. J Neurosurg 81:427–436
55. Ohgaki H, Dessen P, Jourde B, Horstmann S, Nishikawa T, Di Patre PL, Burkhard C, Schuler D, Probst-Hensch NM, Maiorka PC, Baeza N, Pisani P, Yonekawa Y, Yasargil MG, Lutolf UM, Kleihues P (2004) Genetic pathways to glioblastoma: a population-based study. Cancer Res 64:6892–6899
56. Bankes SC (2002) Agent-based modeling: a revolution. Proc Natl Acad Sci USA 99(Suppl 3): 7199–7200